

Quantum superposition in ultra-high mobility 2D photo-transport.

Jesús Iñarrea¹

¹*Escuela Politécnica Superior, Universidad Carlos III, Leganes, Madrid, 28911, Spain.*

We investigate the striking properties that magnetoresistance of irradiated two-dimensional electron systems presents when their mobility is ultra-high ($\mu \gg 10^7 \text{ cm}^2 \text{ V}^{-1} \text{ s}^{-1}$) and temperature is low ($T \sim 0.5 \text{ K}$). Such as, an abrupt magnetoresistance collapse at low magnetic field and a resonance peak shift to the second harmonic ($2w_c = w$), w_c and w being the cyclotron and radiation frequencies respectively. We appeal to the principle of quantum superposition of coherent states and obtain that Schrodinger cat states (even and odd) are key to explain magnetoresistance at these extreme mobilities. On the one hand, the Schödinger cat states system oscillates with $2w_c$, thus being responsible of the resonance peak shift. On the other hand, we obtain that Schrödinger cat states-based scattering processes give rise to a destructive effect when the odd states are involved, leading to a magnetoresistance collapse. The Aharonov-Bohm effect plays a central role in the latter, turning even cat states into odd ones. We show that ultra-high mobility two-dimensional electron systems could make a promising bosonic mode-based platform for quantum computing.

PACS numbers:

Two-dimensional electrons systems (2DES) under low magnetic field (B), turn into a structure of coherent states¹ of the quantum harmonic oscillator. The seminal idea of coherent states²⁻⁸ was introduced by Schrödinger⁶ describing minimum uncertainty constant-shape Gaussian wave packets of the quantum harmonic oscillator. When irradiated under B those systems give rise to the well-known microwave-induced resistance oscillations (MIRO)^{9,10} and zero resistance states (ZRS)^{9,10}. We studied these effects based on *the microwave-driven electron orbit model*¹¹⁻¹⁶. Thus, we found that the time it takes a scattered electron to jump between coherent states, or evolution time τ , equals the cyclotron period, $T_c = 2\pi/w_c$ ¹. The rest of scattering processes at different τ do not significantly contribute to the current. In this way, MIRO reveal the presence of coherent states through this value for τ that is hidden in the peculiar positions that MIRO extrema take in experiments^{9,10}. For instance, MIRO minima comply with $w/w_c = (j + 1/4)$, j being a positive integer. This is a universal result irrespective of platform and carrier.

Experimental evidences¹⁷⁻¹⁹ obtained with irradiated ultraclean ($\mu \gg 10^7 \text{ cm}^2/\text{Vs}$) samples of 2D electrons at low T ($T \simeq 0.5 \text{ K}$), show unexpected and striking MIRO features. First, there is an almost complete magnetoresistance, (R_{xx}), collapse at low B , observed also in the dark and well-known as *giant negative magnetoresistance*²⁰⁻²². Second, at high enough radiation power, there is a resonance peak shift from the expected position, $w_c = w$, to the second harmonic $2w_c = w$, as if the system were under double B . The latter is even more intriguing considering that MIRO, although with lower intensity, keep showing up at the usual positions in smaller mobility samples. We explain the above experiments based on one of the most fundamental principles of quantum mechanics: the quantum superposition. In our case the superposition of coherent states giving rise to Schrodinger cat states. According to the latter, ultra-clean 2DES under a constant B can be described by a system of Schrödinger

cat states (even and odd) that oscillate with a frequency double ($2w_c$) than expected considering the applied field (w_c). Thus, on the one hand, the double frequency oscillations explain the magnetoresistance resonance peak shift to $2w_c = w$. On the other hand, we find that the *odd* Schrödinger cat states when involved in scattering processes undergo a destructive process that makes the scattering rate and in turn R_{xx} , vanish. The Aharonov-Bohm effect plays an essential role in the latter, transforming even Schrödinger cat states into odd ones when a phase shift of π is added. Nevertheless, there is still a remanent part of *even* Schrödinger cat states that would be responsible of the experimentally obtained low intensity MIRO. Thus, we conclude that ultra-high mobility 2DES under low B and T , are made up of even and odd Schrodinger cat states and then can become a promising bosonic mode-based platform for quantum computing^{23,24}.

Paradigmatic examples of quantum superposition are the even and odd coherent states. These states are superpositions of two coherent states of equal amplitude but separated in phase by π radians:

$$|\alpha\rangle_{\text{even}} = \frac{1}{2} N_{\text{e}} [|\alpha\rangle + |-\alpha\rangle] \text{ where } N_{\text{e}} = \frac{e^{|\alpha|^2/2}}{\sqrt{\cosh(|\alpha|^2)}}$$

for even coherent states and $N_{\text{o}} = \frac{e^{|\alpha|^2/2}}{\sqrt{\sinh(|\alpha|^2)}}$ for odd coherent states.

The plus sign corresponds to the even states and the minus to the odd ones. The even and odd coherent states can be obtained from the quantum harmonic oscillator ground state with the action of the even and odd displacement operators², $D(\alpha_{\text{even}})$. The wave function for even and odd coherent states then reads, $\psi_{\alpha_{\text{even}}} = \langle x | D(\alpha_{\text{even}}) | \phi_0 \rangle = \frac{1}{2} N_{\text{e}} e^{i\vartheta_{\alpha}} \times$

$$\left[e^{\frac{i}{\hbar} \langle p \rangle x} \phi_0[x - X(0) - \langle x \rangle(t)] \pm e^{-\frac{i}{\hbar} \langle p \rangle x} \phi_0[x - X(0) + \langle x \rangle(t)] \right]$$

where ϕ_0 is the ground state wave function of the quantum harmonic oscillator, $\langle x \rangle(t)$ and $\langle p \rangle(t)$ are the position and momentum mean values respectively⁸, $\langle x \rangle(t) = \sqrt{\frac{2\hbar}{m^*w_c}} |\alpha_0| \cos(w_c t)$ and

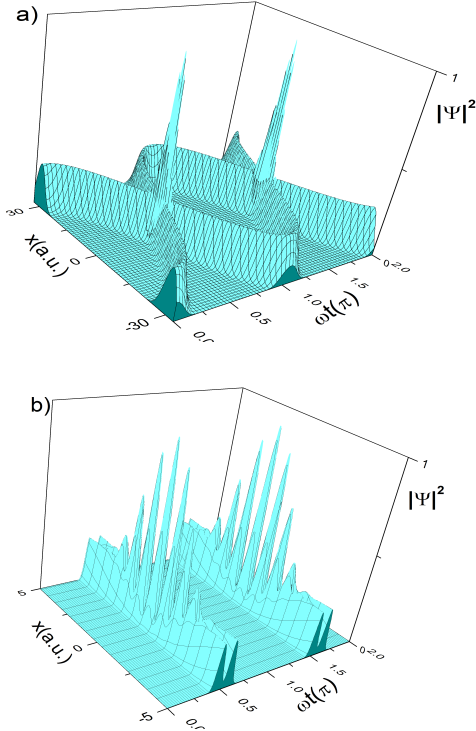


FIG. 1: a) Even coherent state probability density. Quantum interference gives rise to peaks at around $w_c t = \pi/2$ and $3\pi/2$ and $x \sim 0$. b) Zoom-in of the probability density around the peaks. The probability densities shown are based on experimental values^{17,18}.

$\langle p \rangle(t) = -\sqrt{2m^*\hbar w_c}|\alpha_0|\sin(w_c t)$ where we have used that $\alpha = |\alpha_0|e^{-i w_c t}$. When $|\alpha_0|$ is large, as in our case for low B , the coherent states $|\alpha\rangle$ and $|\alpha - \alpha_0\rangle$ can be considered as macroscopically distinguishable. Thus, the above superpositions are referred as *Schrodinger cat states*^{3,4} and then the normalization constants are $N_e \simeq N_o \simeq 1/\sqrt{2}$.

Now we can calculate the probability density of the wave function $\psi_{\alpha}^{(even)}$,

$$|\psi_{\alpha}^{(even)}|^2 = \frac{1}{2} [|\phi_0[x - X(0) - \langle x \rangle(t)]|^2 + |\phi_0[x - X(0) + \langle x \rangle(t)]|^2 \pm 2 \cos\left(\frac{2x\langle p \rangle}{\hbar}\right) \left(\frac{m\hbar}{\pi w_c}\right)^{1/4} e^{-\frac{x^2 + \langle x \rangle^2}{2(\Delta x)^2}}] \quad (1)$$

where the last term gives rise to quantum interference. Thus, both types of superpositions are made up of two Gaussian wave packets oscillating back and forth periodically with a phase difference of π (see Figs. 1 and 2). When they cross, quantum interference shows up and peaks rise. Besides, the system as a whole oscillates with double frequency, $2w_c$. Nevertheless, the most important point is the one of interference. This makes the probability density peaks when $w_c t = \pi/2$ and $3\pi/2$. Thus,

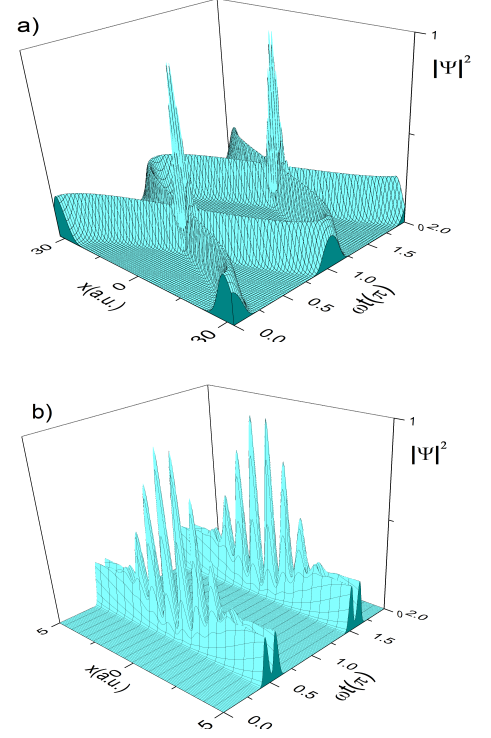


FIG. 2: Same as Fig. 1 for odd coherent states.

we expect that the physical processes of interest, such as electron scattering, will take place mainly at these points.

To calculate R_{xx} we apply a semiclassical Boltzmann model²⁵⁻²⁷, to obtain the longitudinal conductivity σ_{xx} , and then we calculate R_{xx} by the usual tensor relationships^{11,25-27}. Accordingly, σ_{xx} is proportional to the electron-charged impurities scattering rate²⁵⁻²⁷ W_I given by, $W_I = N_i \frac{2\pi}{\hbar} |\langle \psi_{\alpha'} | V_s | \psi_{\alpha} \rangle|^2 \delta(E_{\alpha'} - E_{\alpha})$ where N_i is the number of charged impurities, ψ_{α} and $\psi_{\alpha'}$ are the wave functions corresponding to the initial and final cat states respectively, V_s is the scattering potential for charged impurities²⁵⁻²⁷: $V_s = \sum_q V_q e^{iqx}$, and q_x the x -component of \vec{q} , the electron momentum change during the scattering event. The V_s matrix element is given by²⁵⁻²⁷: $|\langle \psi_{\alpha'} | V_s | \psi_{\alpha} \rangle|^2 = \sum_q |V_q|^2 |I_{\alpha, \alpha'}|^2$. In the scattering rate the essential part is the integral $I_{\alpha, \alpha'}$,

given by,

$$\begin{aligned}
I_{\alpha,\alpha'} &= \int_{-\infty}^{\infty} \psi_{\alpha'}^{(\epsilon)} e^{iq_x x} \psi_{\alpha}^{(\epsilon)} dx = \\
&\frac{N_{(o)}^2}{2} \int_{-\infty}^{\infty} \left[e^{-\frac{ix(\langle p' \rangle - \langle p \rangle)}{\hbar}} e^{-\frac{(x-X'_0 - \langle x' \rangle)^2}{2(\Delta x)^2}} e^{-\frac{(x-X_0 - \langle x \rangle)^2}{2(\Delta x)^2}} \right. \\
&+ e^{\frac{ix(\langle p' \rangle - \langle p \rangle)}{\hbar}} e^{-\frac{(x+X'_0 + \langle x' \rangle)^2}{2(\Delta x)^2}} e^{-\frac{(x-X_0 + \langle x \rangle)^2}{2(\Delta x)^2}} \\
&\pm e^{-\frac{ix(\langle p' \rangle + \langle p \rangle)}{\hbar}} e^{-\frac{(x-X'_0 - \langle x' \rangle)^2}{2(\Delta x)^2}} e^{-\frac{(x-X_0 + \langle x \rangle)^2}{2(\Delta x)^2}} \\
&\left. \pm e^{\frac{ix(\langle p' \rangle + \langle p \rangle)}{\hbar}} e^{-\frac{(x-X'_0 + \langle x' \rangle)^2}{2(\Delta x)^2}} e^{-\frac{(x-X_0 - \langle x \rangle)^2}{2(\Delta x)^2}} \right] dx \quad (2)
\end{aligned}$$

where $\langle p' \rangle(t') = -\sqrt{2m^* \hbar w_c} |\alpha_0| \sin(w_c t')$, $\langle x' \rangle(t') = \sqrt{\frac{2\hbar}{m^* w_c}} |\alpha_0| \cos(w_c t')$ and $t' = t + \tau$. t being the scattering initial time and t' the final scattering time. As we said above, according to the probability density the scattering processes will take place more likely at the probability peaks. Thus, for instance, for the case of $w_c t = \pi/2$ we get to,

$$\begin{aligned}
I_{\alpha,\alpha'} &= e^{iq_x \frac{X'_0 + X_0}{2}} e^{-\frac{q_x^2 (\Delta x)^2}{2}} \times \\
&\left[e^{iq_x \frac{1}{2} \sqrt{\frac{2\hbar}{m w_c}} |\alpha_0| \cos(\frac{\pi}{2} + w_c \tau)} e^{-\frac{[\Delta X_0 + \sqrt{\frac{2\hbar}{m w_c}} |\alpha_0| \cos(\frac{\pi}{2} + w_c \tau)]^2}{8(\Delta x)^2}} \right. \\
&+ e^{-iq_x \frac{1}{2} \sqrt{\frac{2\hbar}{m w_c}} |\alpha_0| \cos(\frac{\pi}{2} + w_c \tau)} e^{-\frac{[\Delta X_0 - \sqrt{\frac{2\hbar}{m w_c}} |\alpha_0| \cos(\frac{\pi}{2} + w_c \tau)]^2}{8(\Delta x)^2}} \\
&\pm e^{iq_x \frac{1}{2} \sqrt{\frac{2\hbar}{m w_c}} |\alpha_0| \cos(\frac{\pi}{2} + w_c \tau)} e^{-\frac{[\Delta X_0 + \sqrt{\frac{2\hbar}{m w_c}} |\alpha_0| \cos(\frac{\pi}{2} + w_c \tau)]^2}{8(\Delta x)^2}} \\
&\left. \pm e^{-iq_x \frac{1}{2} \sqrt{\frac{2\hbar}{m w_c}} |\alpha_0| \cos(\frac{\pi}{2} + w_c \tau)} e^{-\frac{[\Delta X_0 - \sqrt{\frac{2\hbar}{m w_c}} |\alpha_0| \cos(\frac{\pi}{2} + w_c \tau)]^2}{8(\Delta x)^2}} \right] \quad (3)
\end{aligned}$$

Remarkably enough, due to the large value of $|\alpha_0|$ the above expression turns out to be negligible (real exponentials tend to zero¹) except when $\tau = \frac{2\pi}{w_c}$ or $\tau = \frac{2\pi}{2w_c}$. Then, taking this into account, we get to the final expression,

$$\begin{aligned}
I_{\alpha,\alpha'} &= 2e^{iq_x \frac{X'_0 + X_0}{2}} e^{-\frac{[\Delta X_0]^2}{8(\Delta x)^2} - \frac{q_x^2 (\Delta x)^2}{2}} \\
&\pm 2e^{iq_x \frac{X'_0 + X_0}{2}} e^{-\frac{[\Delta X_0]^2}{8(\Delta x)^2} - \frac{q_x^2 (\Delta x)^2}{2}} \quad (4)
\end{aligned}$$

Then, for the even Schrödinger cat states we obtain,

$I_{\alpha,\alpha'} = 4e^{iq_x \frac{X'_0 + X_0}{2}} e^{-\frac{[\Delta X_0]^2}{8(\Delta x)^2} - \frac{q_x^2 (\Delta x)^2}{2}}$ whereas for the odd ones $I_{\alpha,\alpha'} = 0$. We also obtain, not shown, that when one of the scattering-involved cat states, initial or final, is odd the scattering integral is zero too, i.e.,

$$I_{\alpha,\alpha'} = \int_{-\infty}^{\infty} \psi_{\alpha'}^{(\epsilon)} e^{iq_x x} \psi_{\alpha}^{(\epsilon)} dx = 0 \quad (5)$$

At this point is where a geometrical phase shift similar to the Aharonov-Bohm effect comes into play. Starting from an even cat state, ($|\alpha\rangle + |-\alpha\rangle$), we consider that both $|\alpha\rangle$ and $|-\alpha\rangle$, are under the same vector potential \vec{A}

that is taken as constant. Thus, one of the states, say $|\alpha\rangle$, in its motion sees \vec{A} in opposite direction on average (see Fig. 3). However the other state, $|-\alpha\rangle$, that is π radians delayed, displaces with the same direction as \vec{A} giving rise to a phase shift between them. This scenario is similar to the Aharonov-Bohm effect but now B is present in the two wave packet trajectories. Therefore, the individual states $|\alpha\rangle$ and $|-\alpha\rangle$, in their time evolution, after half a cyclotron period T_c jointly complete a circle encompassing a magnetic flux $\Phi = B \times \pi R_c^2$ (see Fig. 3). Where $R_c = l_B \sqrt{2(|\alpha|^2 + 1/2)^8}$, l_B being the magnetic length, $l_B = \hbar/eB$. Thus, the relative geometrical phase shift acquired is $\Delta\phi = \frac{e}{\hbar} \oint \vec{A} \cdot d\vec{r} = 2\pi\Phi/\Phi_0$ where $\Phi_0 = e/h$ is the flux quantum. Then the Schrödinger cat state becomes $|\alpha\rangle + e^{i\Delta\phi} |-\alpha\rangle$. Considering that $|\alpha|^2 = \langle n \rangle$, n being a positive integer (Landau level index), a straightforward calculation leads us to $\Delta\phi = 2\pi\langle n \rangle + \pi$. Thus, $\Delta\phi$ is independent of the magnetic field intensity in turn of Φ . This result contrasts to the Aharonov-Bohm effect where the shift depends on Φ . Accordingly, after $T_c/2$ an even state turns into an odd one and viceversa. Therefore, over a complete oscillation the Schrödinger cat state is half of the time even and half of the time odd alternating the parity. Then, if the cat states scatter when in the odd half of the oscillation, the scattering suffers a destructive interference effect. In the same way as when the state scatters in the even part but ends up in an odd state. In a stationary scenario such processes give rise to the R_{xx} collapse as experiments show.

Thus, quantum superposition and quantum interference along with a phase shift (similar to the Aharonov-Bohm effect) are essential to explain the abrupt R_{xx} collapse in ultra-high mobility 2DES. But further than that, we can identify a novel bosonic mode-based platform to realize robust even and odd Schrödinger cat states: the ultra-high mobility 2D electron systems at low B . Taking all the above into account, the Schrodinger cat states-based magnetoresistance of 2DES can be theoretically described by individual $2w_c$ -coherent states with two τ values, $\frac{2\pi}{2w_c}$ and $\frac{2\pi}{w_c}$. This has to be reflected in their scattering-dependent physical properties such as MIRO. Then, applying the microwave-driven electrons orbits model^{11,12} to this novel scenario¹ we obtain an expression for the irradiated R_{xx} given by,

$$R_{xx} \propto \frac{eE_o}{m^* \sqrt{(2w_c)^2 - w^2}^2 + w^2 \gamma^2} \left(\sin w \frac{2\pi}{w_c} + \sin w \frac{2\pi}{2w_c} \right) \quad (6)$$

The sum between brackets in the R_{xx} expression is made up of two contributions. The first corresponds to $\tau = \frac{2\pi}{w_c}$ and then the cat state parity is conserved during the scattering. The second part corresponds to $\tau = \frac{2\pi}{2w_c}$, and accordingly, during scattering the parity changes from even to odd or from odd to even, giving a null scattering integral. Thus the second contribution can be ruled out and the R_{xx} expression finally reads, $R_{xx} \propto \frac{eE_o}{m^* \sqrt{(2w_c)^2 - w^2}^2 + w^2 \gamma^2} \left(\sin w \frac{2\pi}{w_c} \right)$. This expres-

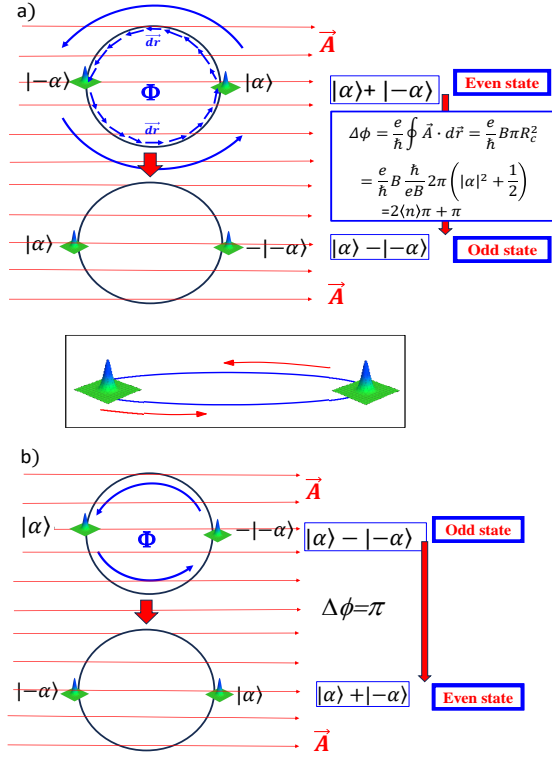


FIG. 3: a) Schematic diagram of the even to odd Schrödinger cat state transition based on a phase shift. b) Same as in a) for the odd to even transition. Inset shows an even or odd Schrödinger cat state, with the two Gaussian wave packets with a delay of π radians. For both panels, the circles correspond to the classical trajectories followed by the two wave packets of the Schrödinger cat states.

sions explains first the resonance peak shift with the amplitude denominator and the MIRO extrema positions with the sine term. Recall the current is held only by even states under irradiation and in the dark .

We can extend the above theory to Schrodinger cat states with three components²⁸ with a state expression that reads: $|\alpha_3\rangle = \frac{1}{\sqrt{3}} [|\alpha\rangle \pm |e^{i2\pi/3}\alpha\rangle \pm |e^{i4\pi/3}\alpha\rangle] = \sqrt{3}e^{-|\alpha|^2/2} \sum_n \frac{\alpha^{3n}}{\sqrt{(3n)!}} |\phi_{3n}\rangle$ with an energy of $E_{3n} = \hbar\omega_c(3n + 1/2)$ and an energy difference between levels of $\Delta E_{3n} = 3\hbar\omega_c$. Therefore, one out of three levels is populated. We can obtain the expression of the wave function similarly as the two component cat state giving:

$$\begin{aligned} \psi_{\alpha_3}(x, t) = & \frac{1}{\sqrt{3}} e^{i\vartheta\alpha} [e^{\frac{i}{\hbar}\langle p \rangle(t)x} \phi_0[x - X(0) - \langle x \rangle(t)] \\ & \pm e^{-\frac{i}{\hbar}\langle p_1 \rangle(t)x} \phi_0[x - X(0) + \langle x_1 \rangle(t)] \\ & \pm e^{-\frac{i}{\hbar}\langle p_2 \rangle(t)x} \phi_0[x - X(0) + \langle x_2 \rangle(t)]] \quad (7) \end{aligned}$$

where $\langle x_1 \rangle(t)$ and $\langle x_2 \rangle(t)$ have similar expression to $\langle x \rangle(t)$ with a phase difference of $2\pi/3$ and $4\pi/3$ respectively. Similar conditions apply to $\langle p_1 \rangle(t)$ and $\langle p_2 \rangle(t)$ regarding $\langle p \rangle(t)$. Accordingly we calculate the probab-

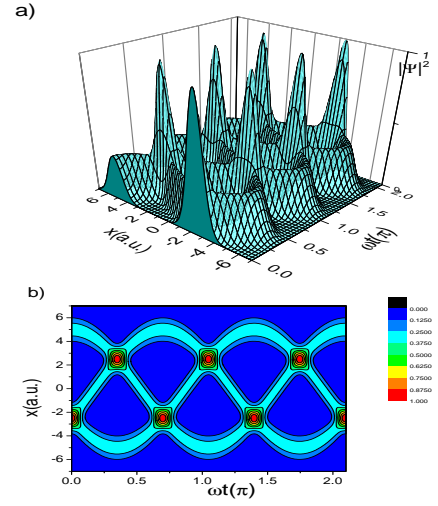


FIG. 4: a) Probability density of a three component Schrodinger cat state. b) Contour plot of the state in a).

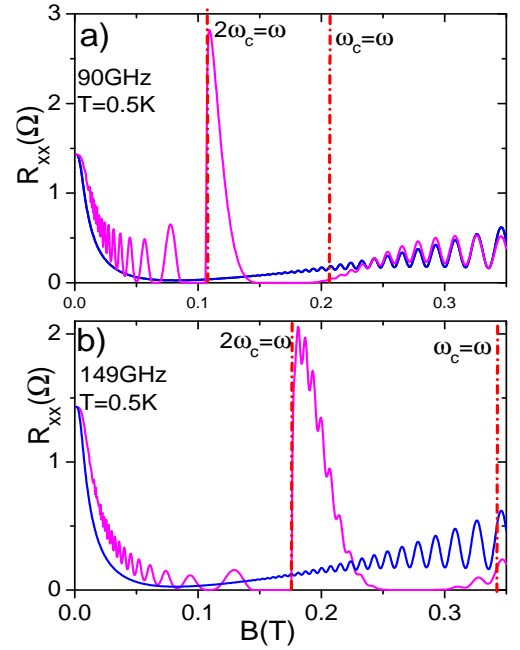


FIG. 5: a) Calculated magnetoresistance vs B for two-component cat states. The radiation frequency is 90 GHz and $T = 0.5 K$ (magenta curve). We also exhibit dark magnetoresistance (blue curve). When radiation is on, the curve shows MIRO, zero resistance states and the rise of a shifted resonance peak at $2\omega_c = \omega$. b) Same as in a) for a radiation frequency of 149 GHz

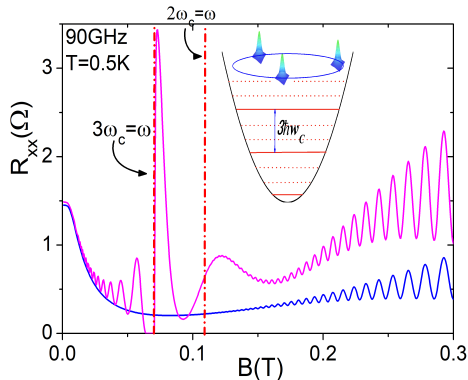


FIG. 6: Calculated magnetoresistance vs B for three-component cat states. The radiation frequency is 90 GHz and $T = 0.5$ K. Dark magnetoresistance (blue curve) is also exhibited. The irradiated curve (magenta curve) shows MIRO, zero resistance states and the rise of a shifted resonance peak at $3w_c = w$. Inset shows a schematic diagram of a three-component cat state.

ity density obtaining interference terms that peak now at $w_c t = 0, \frac{\pi}{3}, \frac{2\pi}{3}, \frac{3\pi}{3}, \frac{4\pi}{3}, \frac{5\pi}{3}$ and 2π (see Fig. 4). We observe that the system now oscillates with $3w_c$. Similarly as the even and odd cat states, we calculate with a semiclassical Boltzman model dark and irradiated R_{xx} . After similar algebra as before, we obtain that R_{xx} is negligible except when τ is given by, $\tau = \frac{2\pi}{3w_c}, \frac{4\pi}{3w_c}$ and $\frac{6\pi}{3w_c}$. Remarkably enough, when irradiated we obtain a resonance peak shift at $3w_c = w$, but still keeping MIRO

their usual positions (see Fig. 6). This is what would be observed in MIRO experiments with even higher mobility ($\mu \sim 10^8 \text{ cm}^2 \text{ V}^{-1} \text{ s}^{-1}$) samples.

In Fig. 5, we exhibit calculated results for dark and irradiated R_{xx} vs B of a two-component cat state. The radiation frequency is (a) 90 GHz and (b) 149 GHz at $T = 0.5$ K. The curves show a surprising strong R_{xx} collapse or giant negative magnetoresistance. When radiation is on, the curves also show MIRO and ZRS, but the most striking effect is the rise of a shifted resonance peak at $2w_c = w$ instead of the expected position, $w_c = w$. However, MIRO extrema show up at the usual positions in agreement with MIRO experiments with lower mobility samples. Another interesting result regarding the peak is the distorted profile it presents that never shows up well-centered in agreement with experiments. In Fig. 6 we present similar results as in Fig. 5a, for a three-component cat state. Now the resonance peak rises at $3w_c = w$.

Summing up, we have introduced the quantum superposition of coherent states giving rise to Schrodinger cat states (even and odd) for ultra-high mobility samples. Based on them, we have explained the experimentally obtained magnetoresistance resonance peak shift to $2w_c = w$. In the same way, we have explained the dramatic magnetoresistance drop that shows up in this kind of samples, irradiated or in the dark. We have generalized the model introducing three-component Schrodinger cat states and predicted that the resonance peak will further shift to $3w_c = w$. Finally, we have proposed, ultra-high mobility 2DES under low B and T , as a promising bosonic mode-based platform for quantum computing.

This work was supported by the MCYT (Spain) grant PID2023-149072NB-I00.

- ¹ Jesus Inarrea and Gloria Platero, Phys. Rev. Res. **6**, 13340, (2024).
- ² V.V. dodonov, J. Opt. B:Quantum Semiclass. Opt. **4**, R1, (2002).
- ³ B. Yurke and D. Stoler, Phys. Rev. Lett. **57** 13 (1986).
- ⁴ Michael W. Noel and C.R. Stroud, Phys. Rev. Lett. **77** 1913 (1996).
- ⁵ V.I. Man'ko *Theory of nonclassical states of light*. Chap. 4. Taylor and Francis. London and NewYork.
- ⁶ E. Srodinger, Die Naturwissenschaften, **14**, 664, (1926).
- ⁷ R.J. Glauber, Phys. Rev. **131**, 2766, (1963)
- ⁸ Claude Cohen-Tannoudji, Bernard Diu, and Franck Laloë, *Quantum Mechanics*.. Wiley and sons. Paris.
- ⁹ R.G. Mani, J.H. Smet, K. von Klitzing, V. Narayanamurti, W.B. Johnson, V. Umansky, Nature **420** 646 (2002).
- ¹⁰ M.A. Zudov, R.R. Lu, N. Pfeiffer, K.W. West, Phys. Rev. Lett. **90** 046807 (2003).
- ¹¹ J. Inarrea and G. Platero. Phys. Rev. Lett. **94** 016806, (2005).
- ¹² J. Inarrea, Sci. Rep. **7**, 13573, (2017).
- ¹³ E.H. Kerner, Can. J. Phys. **36**, 371 (1958) .
- ¹⁴ K. Park, Phys. Rev. B **69** 201301(R) (2004).

- ¹⁵ J. Inarrea, J. Appl. Phys. **113**, 183717 (2013).
- ¹⁶ J. Inarrea and G. Platero, Phys. Rev. B, **84**, 075313 (2011).
- ¹⁷ A. T. Hatke, M. A. Zudov, L. N. Pfeiffer and K. W. West, Phys. Rev. B **83**, 121301(R) (2011).
- ¹⁸ Yanhua Dai, R. R. Du, L. N. Pfeiffer and K.W. West, Phys. Rev. Lett. **105**, 246802 (2010).
- ¹⁹ V. A. Volkov and A. A. Zabolotnykh, Phys. Rev. B **89**, 121410(R) (2014).
- ²⁰ L. Bockhorn, P. Barthold, D. Schuh, W. Wegscheider, and R.J. Haug, Phys. Rev. B. **83** 113301 (2011).
- ²¹ R. G. Mani, A. Kriisa and W. Wegscheider, **3** 2747 (2013).
- ²² J. Inarrea, EPL, **106** 47005 (2014).
- ²³ R.L. de Matos Filho and W. Vogel, Phys. Rev. Lett. **76**, 608, 1996.
- ²⁴ J. I. Cirac, M. Lewenstein, K. Mølmer, and P. Zoller, Phys. Rev. A **57**, 1208, 1998.
- ²⁵ B.K. Ridley. *Quantum Processes in Semiconductors*, 4th ed. Oxford University Press, (1993)
- ²⁶ T. Ando, A. Fowler and F. Stern, Rev. Mod. Phys. **54**, (1982).
- ²⁷ B.M. Askerov, *Electron Transport Phenomena in Semiconductors*., World Scientific, (1994).

- Journal of Physics: Condens. Matter, **27** 415801 (2015)
- ²⁸ B. Vlastakis, et al. Science. **342** 607–610 (2013)